Ultrathin Co films on flat and vicinal Cu(111) surfaces: per atom determination of orbital and spin moments

2003 J. Phys.: Condens. Matter 15 S573

(http://iopscience.iop.org/0953-8984/15/5/311)

INSTITUTE OF PHYSICS PUBLISHING JOURNAL OF PHYSICS: CONDENSED MATTER

J. Phys.: Condens. Matter **15** (2003) S573–S586 PII: S0953-8984(03)57338-6

Ultrathin Co films on flat and vicinal Cu(111) surfaces: per atom determination of orbital and spin moments

A Hahlin[1], J Hunter Dunn[2], O Karis[1], P Poulopoulos[3,4], R Nünthel[3], J Lindner[3] and D Arvanitis[1]

[1] Department of Physics, Uppsala University, Box 530, SE-751 21 Uppsala, Sweden
[2] MAX Laboratory, Box118, SE-221 00 Lund, Sweden
[3] Institut für Experimentalphysik, Freie Universität, Arnimallee 14, D-14195 Berlin-Dahlem, Germany

E-mail: anders.hahlin@fysik.uu.se

Received 11 December 2002
Published 27 January 2003
Online at stacks.iop.org/JPhysCM/15/S573

Abstract

We have performed x-ray magnetic circular dichroism, x-ray resonant magnetic scattering and scanning tunnelling microscopy measurements on ultrathin Co films deposited on flat and vicinal Cu(111). The range of film thickness varies between one and 25 monolayers. For the vicinal Cu(111), Co deposition below one monolayer leads to the formation of elongated islands preferentially oriented along the step edges. These islands extend over lateral length scales of up to several thousand ångströms. For the thicker films we still observe that the vicinal surface leads to the occurrence of a preferential uniaxial growth direction. No such preferential growth direction can be identified for the flat surface. In correlation to the Co growth we observe an increase of both the orbital and the spin moment per Co atom on vicinal Cu(111) of about 25% versus what was observed for Co on flat Cu(111). This enhancement is observed in both the x-ray absorption and the reflectivity measurements. Similar to what was earlier reported for Co on Cu(100) we also observe for the case Co on Cu(111) an increase in the ratio m_l/m_s (orbital to spin moments) of 40% for thin Co films. In contrast to what has been reported for Co films on flat and vicinal Cu(100) we do not observe any major variations in the occupancy of the Co 3d states for Co grown on the vicinal Cu(111) surface.

(Some figures in this article are in colour only in the electronic version)

1. Introduction

During the last decade new skills for growing and studying *in situ* ultrathin films were developed. Epitaxial ultrathin films, bilayers and superstructures were grown by techniques

[4] Present address: Materials Science Department, University of Patras, 26504 Patras, Greece.

such as electron beam evaporation, molecular beam epitaxy (MBE) and sputtering techniques. This has led to a rapid increase in thin-film research, with many interesting technical applications as an output, such as magnetic sensors and new storage media. Recently, the trend has been to decrease the lateral thin-film dimensions, aiming at magnetic nano-structures, such as small magnetic particles or magnetic wires. These materials often exhibit magnetic characteristics strongly different from what is found in the bulk (or even at the surface). One way of preparing such materials is to introduce artificial nano-structures already at the substrate surface. A promising method of producing magnetic wires is to make use of vicinal (high-index) surfaces, forcing the magnetic material to grow along the surface terraces.

De la Figuera *et al* [1] claimed to have fabricated magnetic 'quantum wires' by means of thermal deposition of Co on a vicinal Cu(111) single-crystal surface. The samples were studied by scanning tunnelling microscopy (STM) and did indeed show wire formation along the (110) direction. Scanning electron microscopy (SEM) studies with polarization analysis were performed by Berger *et al* [2] for Co on vicinal Cu(100) clearly showing that the easy axis of magnetization is parallel to the direction of the step edges. Later, Kawakami *et al* [3] showed, by performing surface magneto-optic Kerr effect measurements, that the step-induced anisotropy of Co on vicinal Cu(100) depends linearly on the step density, and exists already for small vicinal angles, that is, vicinal angles below 1°, corresponding to terrace widths of the order 150–200 Å.

In an x-ray magnetic circular dichroism (XMCD) study, Tischer *et al* [4] showed that the orbital magnetic moment m_l for Co films grown on Cu(100) is enhanced by 40% for ultrathin films compared with the bulk value. Later, Dürr *et al* [5] did a similar investigation for Co grown on a vicinal Cu(100) single-crystal surface and found a 200% increase of m_l for the ultrathin film. The authors concluded this finding as a correlation between the step induced anisotropy and the orbital magnetic moment. Furthermore, it was suggested that the enhancement was due to symmetry breaking in the surface layer caused by the introduction of atomic steps.

We report on XMCD and resonant x-ray reflectivity magnetic scattering (XRMS) measurements of ultrathin Co films deposited on a flat and vicinal Cu(111) single crystal. Our aim here is to obtain a better understanding of how electronic and magnetic properties evolve when moving from a quasi-one-dimensional nano-structure to a one-dimensional thin film. We therefore also performed on the same crystal STM experiments to characterize the growth on the Co films. Spectroscopic methods based on the use of synchrotron radiation are excellent tools to examine such dilute systems. X-ray absorption (XA) spectroscopy, where the tunability of the photon energy is utilized, provides element specific electronic structure information on unoccupied electronic states, and is sensitive even for small changes in, e.g., elemental or structural composition. At synchrotron radiation facilities, where special sources provide circularly polarized x-rays, the technique of XMCD may be used. XMCD provides us with element specific information of the orbital and spin magnetic moments by making use of magneto-optic sum-rules [6]. The moment values can be normalized on a per atom basis. No knowledge of the amount of Co is necessary to obtain such *per atom* information. A correlation of the spectroscopic with the STM results allows us to examine how the real space morphology at the mesoscopic length scales influences the magnetism.

2. Experimental details

The XA and XRMS measurements were performed at beam-line 5.2 of the Stanford Synchrotron Radiation Laboratory (SSRL). The photon energy resolution was better than 1.5 eV at the Co $L_{3,2}$ edges. This beam-line is based on an elliptically polarizing undulator

(EPU), which enables the state of the polarization to be varied. A specially cut Cu(111) single crystal was used, presenting both a flat and a vicinal region. This crystal enabled us to record XA and XRMS spectra from both regions within the same sample preparation. All samples were prepared and measured under ultrahigh-vacuum (UHV) conditions. The crystal surfaces were cleaned and prepared by cycles of argon ion beam sputtering followed by annealing to 900 K. These cycles were repeated until no traces of contamination could be detected by means of XA spectroscopy. As a rule of thumb, this implies that fewer than $1/100$ of the atoms in the surface region are contaminants. The order of the surface structure was checked by means of low-energy electron diffraction (LEED). Co was deposited at room temperature by means of electron beam evaporation at the rate of 0.5 monolayers (ML) Co min^{-1}. The film thickness was determined from the edge jump ratio in the XA spectra. This calibration method is described in detail by Arvanitis *et al* [7]. The characterization of the crystal surface structure and the Co initial growth were performed *in situ* in a similar UHV chamber by using STM [8]. The same recipe for cleaning as described above was used. The various Co films were prepared at a pressure of about 5.5×10^{-10} mbar. The STM experiments were performed at room temperature and the images were recorded in the constant current mode. The flat part of the Cu crystal shows terraces of about 300 Å. The analysis of several STM images taken on the vicinal part revealed a miscut of 1.25° which results in a mean terrace width of about 110 Å and steps running along the [110] direction. The XA measurements were performed in the total electron yield mode. Both a multi-channel plate (MCP) detector and the sample drain current were used to monitor the yield. These channels were typically found to generate identical results. The experimental set-up enables the rotation of the sample independently of rotation of the coils for magnetization. The samples were magnetized using pulses of 180 Gauss in the easy direction and measured at zero magnetic field.

The sample is positioned in such a way that at 0° x-ray grazing incidence $\boldsymbol{k}$ lies along the $[1\bar{1}0]$-direction, that is, along the step edges for the vicinal face. The spectra are dominated by $2\mathrm{p}_{3/2,1/2} \rightarrow 3\mathrm{d}$ transitions which can be viewed as imaging the density of the 3d unoccupied states [9]. By making use of circularly polarized x-rays in the XA process we obtain this information in a spin selective fashion. This is the basis for the XMCD technique [6, 10].

The photon energy dependent atomic scattering factor $f(E)$ can be described as consisting of two parts: an imaginary part (absorptive part) and a real part (reflective part)

$$f(E) = f_0 + f'(E) + \mathrm{i}f''(E) \tag{1}$$

where f_0 is the energy independent part of the atomic scattering factor. Thus, to gain full information on the scattering process both the absorptive and the reflective part of the x-ray interaction must be recorded. The XRMS data for this investigation were obtained by recording, simultaneously with the electron yield, the total reflected intensity with a photo-diode positioned at an angle of 2θ, where θ is defined as the angle of the sample surface with respect to the incident x-rays. To increase the angular resolution and avoid spurious signals in the reflected intensity a small pinhole (10 μm) was positioned in front of the photo-diode. As in the case for the XA measurements, the spectra are dominated by sharp features coinciding in energy with the $2\mathrm{p}_{3/2,1/2} \rightarrow 3\mathrm{d}$ transitions. With circularly polarized x-rays we can monitor how the scattered intensity depends on the coupling between the sample magnetization and the polarization vector of the x-rays. The magnetic contrast in the reflectivity channel exceeds in magnitude what is seen for XMCD, and thus appears an excellent complementary tool for magnetic investigations. Especially for thicker samples, where XA spectroscopy due to the electron escape depth (λ_e) (for Co $\lambda_e = 17$ Å at this photon energy) just allows for surface information, the probing depth for the x-rays enables magnetic information several hundred ångströms beneath the surface region. However, no straightforward sum rules for XRMS data

have been used in the literature for magnetic moment determination. We note in particular that diffraction effects from the probed Co and Cu region need precise modelling starting from equation (1) [11]. Here we give only a qualitative analysis of the reflectivity data. To obtain the full value of the XMCD and XRMS signals, the samples were cooled when necessary to avoid a reduction of the dichroic signal due to finite-size effects.

The quantities that can be most reliably determined in the XA (such as the XMCD) and x-ray reflectivity (the XRMS signal) modes are not the same. XA is the technique of choice to obtain the ground-state number of 3d holes and the ground-state orbital and spin moments. The XA spectra are mostly measured by means of electron yield detection in the present spectral range. The sample's weak x-ray fluorescence yield can also be used in the presence of sufficiently high photon fluxes. One monitors here the intensity of the secondary channel of choice as a function of photon energy. For this study we use electron yield detection. Either the sample photo-current, total or partial electron yield using a channel plate detector positioned below the sample are recorded. These channels yield signals directly proportional to the atomic cross section of the photo-excited atoms that are probed by the incoming x-rays and visible within the chosen secondary channel's effective probing depth. For electron yield based channels the highest degree of accuracy is achieved in the absence of external applied magnetic fields. This is particularly important in the case of dilute samples such as surfaces and ultra-thin films investigated here. A very high degree of accuracy may be achieved allowing one to reach a sensitivity comparable with that of SQUID magnetometry working under remanent conditions. On the other hand the XRMS channel, based on photon excitation and photon detection, is easily made compatible with external applied magnetic fields at the sample. Unfortunately no simple straightforward data analysis procedure is proposed in the present literature to directly obtain ground-state magnetic moments. One has to apply an indirect procedure based on Kramers–Kronig transformations. If no such indirect analysis is applied, the XRMS channel is therefore often used in a more qualitative way in order to obtain quantities proportional to the total magnetization only, at fixed photon energies, as a function of an external control parameter such as an applied magnetic field. One assumes here that in the absence of a macroscopic magnetization the magnetic contrast in the XRMS signal will vanish. This is a weaker working assumption than for the XAS and XMCD channels where spectral areas are directly linked to physical quantities. The vector character of XMCD, based on the angular momentum transfer of the exciting radiation, is also present in the XRMS channel, allowing for three-dimensional vector magnetometry applications.

3. Results

For Co growth on vicinal Cu(111) the Co islands coalesce into a preferential growth along the step edges with a typical height of 2 ML. As seen in figure 1(a) even for the flat surface at very low Co coverage islands of Co are formed along the step edges. The diameter of these connected islands is about 40 Å (corresponding to 20–25 Co atoms) and the mean step height is about 3 Å. The mean value of the terrace width is larger than 300 Å. In more detail, we observe 53% monatomic, 36% double-atomic and 14% triple-atomic steps. So even this *flat* surface cannot strictly be considered flat as it exhibits steps corresponding to what a surface of a miscut of 0.55° would lead to. However, this is not a directed miscut. On a macroscopic scale these step edges run along various directions and are imperfections that can hardly be avoided. Figure 1(b) shows the initial growth on the vicinal Cu(111) surface. Here the coverage is still very low (well below 1 ML), although somewhat higher than is shown for the flat surface. The preferential growth of the Co islands is found to lie in the same direction with a diameter of about 40 Å. Here we found 75% monatomic, 22% double-atomic and only 3% triple-atomic

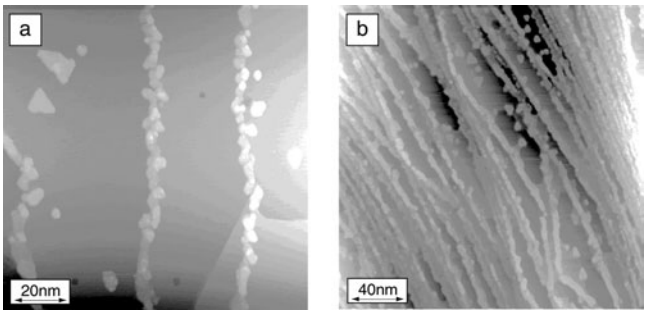

Figure 1. Topographic image of very low Co coverage on flat (a) and vicinal (b) Cu(111). The size of the image is 1200 × 1200 Å and 2500 × 2500 Å for (a) and (b), respectively.

steps. In this case the arithmetic mean of the step height was somewhat lower (2.2 Å) compared to what was observed for the flat case. If the terrace width is larger than the diffusion length, stable islands may be created as is seen in figure 1(a).

At 2 ML Co coverage on the flat Cu(111), see figure 2(a), the surface looks rough and, as already known from other investigators [1, 12], parts of the substrate are still uncovered. More interesting and to our knowledge *not explored systematically until now*, in this thicker range, is the growth on the vicinal surface, see figure 2(b). One can still identify the vicinal morphology with the Co preferentially growing along the $[1\bar{1}0]$ direction with just a few cross links between the Co parts. The roughness is about 2–3 Å (see inset in figure 6) and the Co islands start to coalesce (merge together). As known from previous studies the islands on the flat part start to coalesce at about 5 and at 10 ML; they appear as in figure 3(a). Figure 3(b) shows the corresponding vicinal part which though rough still presents clear and nicely shaped stripelike Co along the step edges. This shows that just a small miscut is needed to stabilize a uniaxial growth direction even at higher Co coverage. The islands on the vicinal surface are smaller than the islands on the flat part along the step edges. This is what one expects intuitively because of the limitation induced by the narrow terraces in one direction. The initial Co growth on Cu(111) was early reported by Gonzalez *et al* [13] to grow in an HCP phase. However, Le Fevre *et al* [14] reported extended x-ray absorption fine-structure (EXAFS) results showing that Co films, for thickness up to 3 ML, grow in a phase of distorted fcc symmetry. Thicker Co films eventually switch to the bulklike HCP stacking. The authors report an in-plane nearest-neighbour (nn) distance of 2.54(1) Å, and the out-of-plane nn distance of 2.50(1) Å for Co films ranging from 1 up to 8 ML. The Cu substrate, which has an nn distance of 2.55 Å, forces the Co atoms to adopt a larger in-plane parameter, parallel to the interface, than in bulk Co. Bulk Co atoms would have an nn distance of 2.51 Å.

In figure 4 we present Co $L_{3,2}$ XMCD and XRMS spectra recorded for a 2.5 ML film deposited on a Cu(111) single-crystal surface. The data were obtained by using circular polarized x-rays, keeping the polarization of the x-rays fixed and switching the remanent magnetization. The sample surface was positioned at an angle of 15° with respect to the direction of the incident x-rays. The lower part of the figure shows the XMCD spectra for Co on the flat and vicinal Cu(111) single-crystal surface. The data are shown after a constant background subtraction followed by setting the post edge, to 100 arbitrary units. Under these conditions the spectra can be directly compared and yield information on a *per atom* basis. We observe a strong modification in the magnetic properties comparing the Co spectra for flat and vicinal surface: the enhancement of the dichroic response scale by 25% for the vicinal surface compared to what is found for the flat surface. An investigation for a similar system, Co on

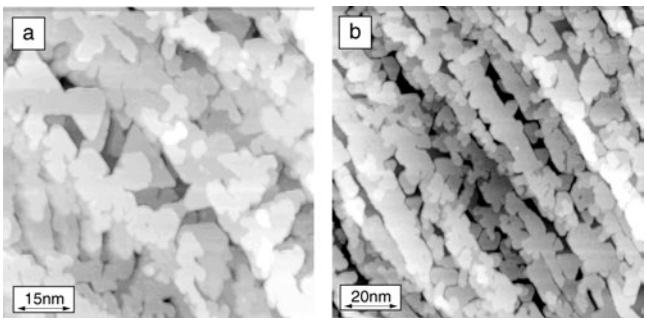

Figure 2. Topographic image of 2 ML Co on flat (a) and vicinal (b) Cu(111). The size of the image is 900 × 900 Å and 1200 × 1200 Å for (a) and (b), respectively.

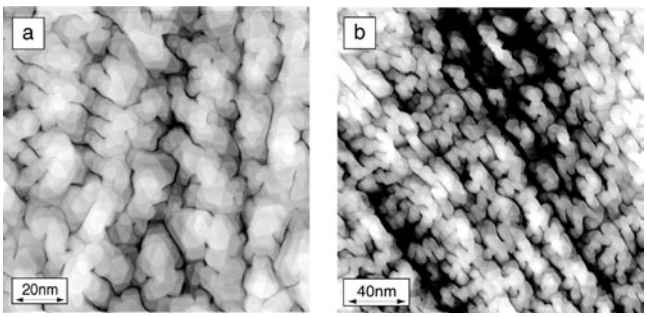

Figure 3. Topographic image of 10 ML Co on flat (a) and vicinal (b) Cu(111). The size of the image is 1200 × 1200 Å and 2000 × 2000 Å for (a) and (b), respectively.

vicinal Cu(100), was reported by Dürr *et al* [5]. By introducing a vicinal Cu(100) single-crystal substrate the authors report strong differences in the Co electronic structure manifest in a narrowing of the L_3 peak and an energy shift of the $L_{3,2}$ peaks as a function of Co coverage for the Co on vicinal Cu(100). In the case for Co on Cu(111), using the present data set, a precise comparison has shown that these effects are not found [15]. Instead, for very thin Co films on the vicinal Cu(111) surface, a broadened L_3 peak was found due to inhomogenous broadening.

In the upper part of figure 4 XRMS spectra from the flat and vicinal surfaces are presented with an offset of 400 arbitrary units. The reflectivity spectra were recorded simultaneously with the XMCD data with a photo-diode detector positioned at the angle of the specular reflection. The XRMS spectra were normalized in such a way that the L_3 peak in the XRMS channel scales in intensity with the L_3 peak in the absorptive channel. No straightforward *per atom* normalization is possible for this channel. As in the case for the absorption measurements we also here observe strong effects in the magnetic contrast when comparing data from the flat and vicinal crystals. Also interesting is the energy location of the $L_{3,2}$ peaks for the XRMS measurements. The L_3 peak appears 0.6 eV lower in energy compared with the L_3 peak in the absorption channel, whereas the L_2 peak is shifted 0.4 eV lower in energy. As the photon energy reaches the maximum of the absorption peaks, the reflected intensity, instead of an increase, decreases rapidly. In the reflectivity channel the reflected intensity is very much dominated by the L_3 transition, whereas the L_2 peak barely is seen. Moreover, significant differences are observed in energies above the L_3 transition in terms of reflected intensity from flat and vicinal surfaces. Both spectra from the flat surface coincide in the pre and post edge whereas the spectra taken for the vicinal surface fall below in intensity.

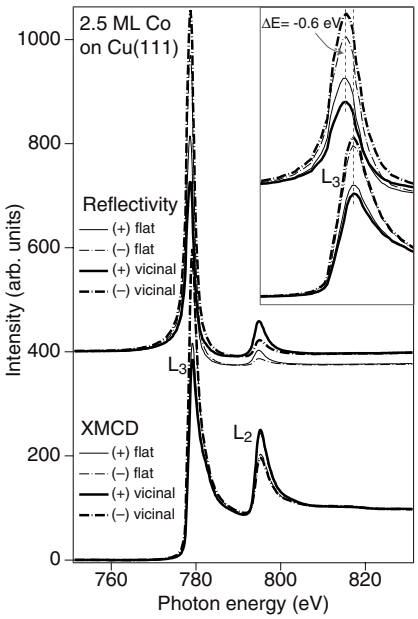

Figure 4. XRMS (upper spectra) and XMCD (lower spectra) data recorded at room temperature from a 2.5 ML Co coverage on the flat and vicinal Cu(111). The inset shows the spectra for the energy region in the vicinity of the L_3 peak. Here we observe an energy shift for the maximum of the reflectivity channel of $\Delta E = -0.6$ eV compared with the location of the L_3 absorption peak.

In figure 5 difference spectra from the XMCD and XRMS data presented in figure 4 are shown. The upper part of figure 5 shows the difference spectra from the absorption experiment which were obtained by subtracting the minority spectra from the majority spectra. Applying the magneto-optic sum rules [6] on these spectra enables the determination of the ratio m_l/m_s. Here the dipolar term has been neglected. To determine the m_l (orbital) and the m_s (spin) moment separately, we have also recorded the isotropic *linear light* spectra and the number of 3d electrons in cobalt. The lower part of figure 5 shows the difference spectra for the XRMS data from figure 4 with an offset of -100 atomic units applied. The differences were obtained by subtracting the minority spectra from the majority spectra. The magnitude of the magnetic response for the Co is 100% stronger for the vicinal surface compared with the flat surface. This cannot however be straightforwardly interpreted as an increase of 100% in the magnetic moment as XMCD and XRMS cannot be easily compared. When comparing the difference spectra from the XMCD and XRMS measurements we observe that in the case of XRMS the strongest magnetic effects are found in the vicinity of the L_3 transition whereas the signal at the L_2 transition is very weak.

In figure 6 we present the most reliable quantity we may obtain experimentally: the ratio between orbital and spin moment (m_l/m_s) for a range of thickness of cobalt films deposited on flat and vicinal Cu(111). We also present experimental results and theoretical predictions for m_l/m_s for the Co/Cu(100) system earlier reported by Tischer *et al* [4]. At high coverage m_l/m_s is constant around the bulklike value of $\approx$0.08 for both flat and vicinal Cu(111). As in the case for ultrathin Co on Cu(100), we here observe an increase in m_l/m_s of about 40% for both the vicinal and flat surface when decreasing the thickness of Co. Tischer *et al* addressed the enhancement of m_l/m_s for thin Co on Cu(100) by the lowering of the symmetry at the surface, so that the first Co layer would correspond to an orbital moment of 0.26 μ_B/atom.

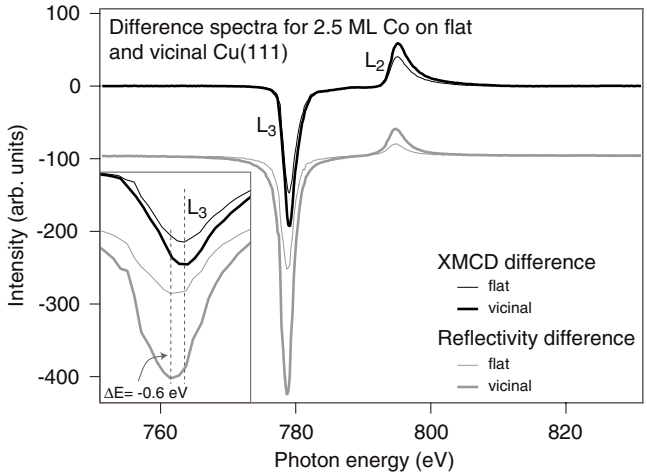

Figure 5. XRMS and XMCD difference data recorded at room temperature from a 2.5 ML Co coverage on the flat and vicinal Cu(111). The upper spectra represent difference spectra for the XMCD spectra whereas the lower the difference spectra for the XRMS data with an offset of −100. The inset shows the spectra in the vicinity of the L_3 energy interval.

The introduction of the vicinal surface would then ideally further decrease the symmetry, with a higher order of the ratio *surface to bulk* atoms as a consequence. Interesting is that both flat and vicinal Cu(111) follow the same trend, and no supplementary *step induced* increase is found here in m_l/m_s in contradiction to what was reported for the Co on Cu(100) [5]. At first glance this is surprising, since one might expect that on the vicinal surface a larger number of surface atoms is located at step edges, thus leading to a higher value of m_l. A detailed investigation of the STM images gives the possibility of estimating the relative number of surface to bulk atoms.

We first discuss the low-coverage regime and start with the number of step edge atoms on the bare Cu(111) surface. As already pointed out the experimentally found values for the mean terrace width are about 110 Å for the vicinal and 300 Å for the flat part. Taking the distance between the atomic rows of 2.2 Å perpendicular to the step edges (along the $[11\bar{2}]$-direction), this means that the typical terraces for the vicinal part consist of 50 atomic rows for the vicinal and 135 atomic rows for the case of the flat part. Then, the number of step edge atoms having three nearest neighbours relative to 'normal' surface atoms which have six nearest neighbours is 2% for the vicinal and 0.7% for the flat surface. In the first stage of the Co deposition, for thicknesses smaller than 1.5 ML, our STM measurements show in accordance with the literature that the systems mainly grow via step flow growth, decorating the step edges with 2 ML high Co wires (see figure (1)). Only on the larger terraces are triangular islands formed. In this growth regime, each Co wire contributes with two edges running along the steps to the number of step edge atoms. Neglecting in a first approximation the step edge atoms due to the formation of islands, the values for the number found experimentally on the bare Cu surfaces should be simply multiplied by a factor of two, i.e. for low Co coverage 4% step edge atoms are expected on the vicinal, whereas 1.4% are expected on the flat part. This estimation is in good agreement with values found on typical STM pictures, where numbers of 4% for the vicinal and 2.3% for the flat part are derived. The small increase on the flat part can be attributed to the larger number of islands observed there, which for the estimation have been neglected. The fact that the islands contribute much less to the overall number of step edge atoms compared

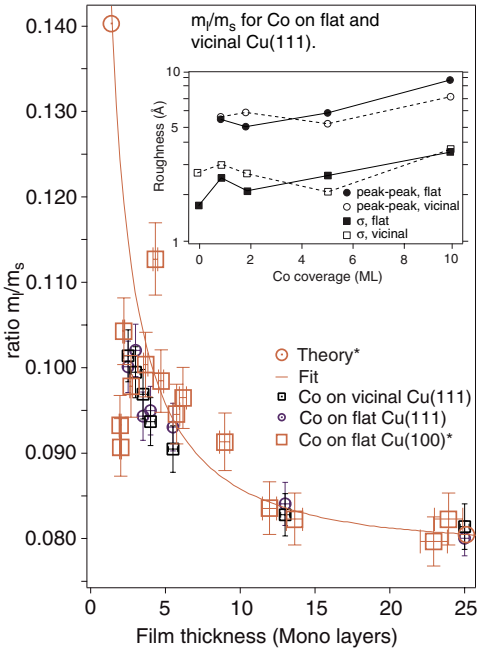

Figure 6. Ratio of orbital and spin moment (m_l/m_s) versus Co thickness. The squares and the circles represent m_l/m_s obtained for Co on vicinal Cu(111) and flat Cu(111) respectively. The filled squares represent m_l/m_s for Co on Cu(100). The filled circles are calculated points for m_l/m_s for Co on Cu(100) [4] and the solid curve represents a thickness dependent model fit taking into account the contribution from surface and bulk atoms, respectively [4].

to the Co wires can be understood, since at room temperature we find an increase in size of the islands upon increasing the Co coverage rather than an increase in the island density. When one then considers that the number of edge atoms within a triangular island increases only as $\sqrt{A}$, where A is the island area, it is clear that the main contribution arises from the Co wires. For the low-coverage regime one has to conclude that the difference in the ratio of step edge to surface atoms is very small.

Now we discuss the coverage regime above 1 ML. From the STM analysis we can quantify the roughness for several thicknesses of Co on the substrate by means of the root mean square (σ). This is presented in the inset of figure 6. The filled and open squares represent the roughness for Co on the flat and vicinal Cu(111), respectively. The quantity σ is defined as the standard deviation of the height levels relative to a reference plane with a height $\bar{z}$:

$$\sigma = \sqrt{\frac{1}{N}\sum_{i=1}^{n}(z_i - \bar{z})^2}, \tag{2}$$

where

$$\bar{z} = \frac{1}{N}\sum_{i=1}^{n} z_i. \tag{3}$$

The z_i represent the height at position i. The roughness for both the flat and vicinal parts is already within the first ML around 2–3 Å, and does not vary significantly for higher coverage. In addition, the terrace width shows a coverage dependence. For the Co grown on the flat part the terrace width decreases monotonically, whereas for the case of the vicinal substrate a local

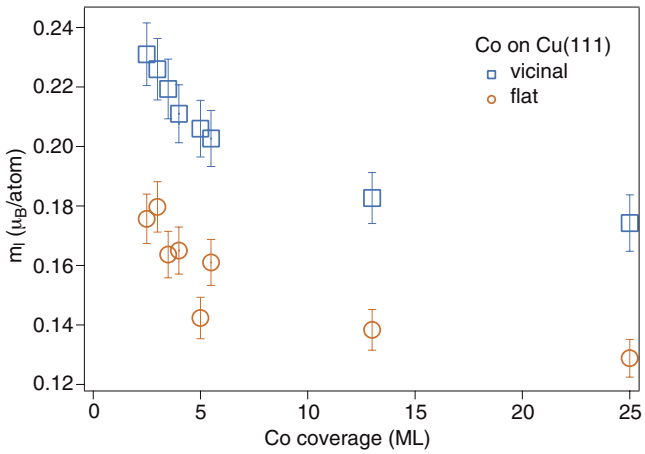

Figure 7. Orbital moment versus Co coverage. The squares and the circles represent the Co coverage dependent orbital moments for Co on vicinal and flat Cu(111) respectively.

minimum is a observed at 1 ML of cobalt. This is attributed to the formation of elongated Co islands at this coverage. The upper part of the inset shows the peak-to-peak roughness for the two surfaces. However, similar to σ, the maximum roughness also shows only small changes with the introduction of the vicinal Cu(111). Thus, the surfaces exhibit comparable roughness and therefore the ratio of step edge to surface atoms is not dominated by the existence of the stripelike Co growth but rather by the roughness of the whole film, which is very similar on the two surfaces. The structural findings go along with the observation that m_l/m_s does not vary when comparing flat and vicinal Cu(111). In other words, introducing atomic steps in the Cu(111) substrate, that is, forcing the Co film growth from a two-dimensional (2D) towards a one-dimensional-(1D-) like growth, does not affect the ratio m_l/m_s but nevertheless enhances both the orbital and spin moment per Co atom separately.

In figures 4 and 5 normalized XMCD, XMRS and difference spectra are shown for a 2.5 ML Co film deposited on flat and vicinal Cu(111). When applying the magneto-optic sum rules on these XMCD spectra we obtain values for the spin moment m_s of 1.6 and 2.0 μ_B/atom for Co on flat and vicinal Cu(111), respectively. We find that these values for the spin moment are constant for the whole thickness range even for films at relatively high coverage (25 ML). In figure 7 the orbital moment (m_l) versus Co coverage is shown. The circles and the squares represent m_l per atom for Co on flat and vicinal Cu(111), respectively. The enhancement of m_l with the decreasing Co coverage is correlated to the ratio *surface to bulk* atoms and is found for both the Co on vicinal and flat Cu(111) systems. However, an increase of about 25% in m_l for the vicinal system is observed for the whole thickness range. As just discussed this additional enhancement cannot be correlated to the ratio *surface-to-bulk* atoms; it can then tentatively be correlated with the fact that the Co atoms grow along a preferential direction.

4. Discussion

The fact that a preferential growth direction is still present indicates that the introduction of the vicinal surface still plays a role for thicknesses at 25 ML. A possible cause for the higher moment for the vicinal surface could be the introduction of strain related to the uniaxial island formation. However, this explanation alone is not satisfactory due to the fact that the

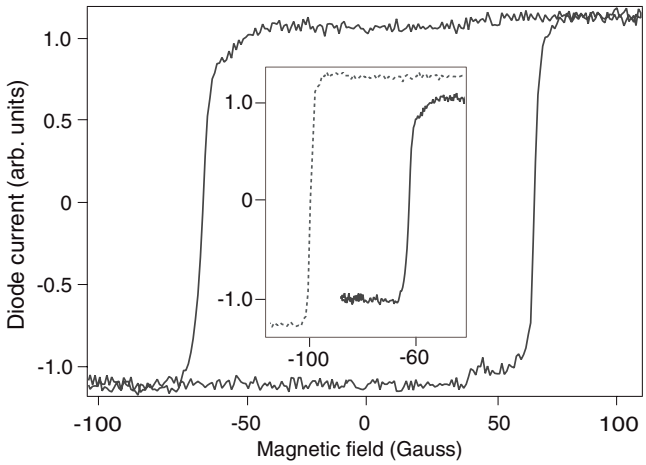

Figure 8. Hysteresis measurements for 25 ML Co on flat Cu(111) (solid curve). The data were recorded at room temperature *in situ* during the synchrotron radiation based work. The time to scan the magnetic field (200 G) is about 2 min. The photon energy is set at the XRMS L_3 maximum (see figure 4), and the magnetic field is then scanned. We observe that the full saturation value is obtained at remanence. In the inset the magnetization reversal of both the flat and the vicinal film (dashed curve) for the same thickness is shown. We observe a stable remanence but also a higher coercive field in the case of the vicinal film.

step induced anisotropy on a similar system, Co on Cu(100), depends linearly on the step density [3]. To ensure that the magnetic moment enhancement is not just an artifact of a tilted easy direction of the flat versus the vicinal surface, hysteresis curves were taken in the reflectivity channel. These curves, shown in figure 8, give further insight into the values of the anisotropy energies. We show the data for a 25 ML film that also exhibits the observed enhancement of the magnetic response for the vicinal case. The experimental set-up is identical with the one described earlier for the XRMS measurements. For this experiment the photon energy is constant and set such that dichroic contrast is observed at the L_3 edge in the reflectivity mode (see XRMS figure 4). The applied magnetic field value is then varied slowly. For the vicinal surface the magnetic field is oriented along the step edges. The data of figure 8 indicate a mostly square hysteresis loop for the flat surface (solid curve). We therefore conclude that for the flat surface there is no loss of remanence due to a multiple domain breakdown or a coherent magnetization rotation to a different direction. In the inset of figure 8 a comparison of the magnetization reversal is shown for the flat and vicinal surfaces for this Co thickness. Here the reflected x-ray signal is recorded, as the magnetic field strength applied opposite to the direction of the remanent magnetization is slowly increased. For the vicinal case (dashed curve) a steplike reversal is also observed leading to the full saturation value at remanence. The almost square shape indicates again that no loss of remanence is observed, and is consistent with the easy direction being along the step edges as also reported elsewhere [3]. The coercive field, H_c, for the vicinal surface is larger. These measurements were made in parallel with the XMCD measurements presented here under identical conditions. We conclude that for both the flat and vicinal surfaces the magnetic remanence was almost identical with the saturation magnetization. The observed moment enhancement is no artifact due to the specific sample orientation versus the magnetic field direction and magnetic field value.

Of interest is also the implication of the data of figure 8 for the value of the anisotropy constant along the easy direction. To further quantify these results we assume a pure uniaxial

anisotropy energy of second order only, and we use the relation $K = H_c M$. K represents the uniaxial anisotropy constant, and M the magnetization. For M the values for the magnetic moments obtained earlier were used. We obtain, from the data of figure 8, that $K_{step} = 2K_{flat}$. For the present data, as we also know the value of the magnetic moments in μ_B/atom we can furthermore calculate the difference in the anisotropy energy (ΔK), between the vicinal and flat surfaces in the easy direction. We obtain

$$\Delta K = K_{vicinal} - K_{flat} = 5.79 \times 10^{-7} \text{ eV/atom}. \tag{4}$$

As a next step, we can attempt, according to what was shown by Bruno [16], to link this anisotropy energy to the variation of the orbital moment we determined earlier in figure 7. In the simplified linear relation proposed by Bruno we use the scaling factors for Co atoms that were used earlier with success for Co thin films [10]. An orbital moment variation of 0.05 μ_B between the easy and hard magnetization direction would then correspond to a magnetocrystalline anisotropy energy of 1×10^{-4} eV/atom, to be compared with ΔK. The value of 0.05 μ_B is used here as this is the value obtained from the data of figure 7 for the orbital moment increase for the vicinal case for 25 ML. One has to assume that the orbital moment in the surface plane for the flat face is mostly isotropic and the associated magnetocrystalline anisotropy in the surface plane of the flat face is weak. One would then have direct access to the orbital 'step induced' orbital moment anisotropy along the easy direction by considering the difference between the flat and vicinal surface data. We observe that the order of magnitude between the two results is very different indicating that either in the present case the observed 'step induced' anisotropy is not of magnetocrystalline character or that one of the assumptions we use is not fulfilled. A recent XMCD study for FeNi films on vicinal Cu(111) measures the 'step induced' orbital moment anisotropy to be of order 0.1 μ_B leading to even stronger values for the associated magnetocrystalline anisotropy [17]. However, no independent determination of the anisotropy energy, such as in figure 8, is presented for this system. Here we obtain results only along the easy direction and a definite conclusion is not possible as the orbital moment anisotropy also needs to be measured along the hard direction. However, one would need to assume, for the present system, that the orbital moment variation in the hard direction is also varying such that the present enhancement cancels out in order to match the measured value of ΔK. For FeNi on vicinal Cu(111) no simultaneous work on a flat surface is reported to make a full comparison with our present set of data.

In the present context of discussing differences in order of magnitude of anisotropy energies and anisotropy of the orbital moment, as probed by different experimental techniques, it is of interest to situate the present set of data with recent work in the literature [18–20]. Recently it has been claimed that data obtained by means of XMCD and the magneto-optic Kerr effect yield different orders of magnitude of the magnetic anisotropy energy [18]. It is also claimed that the presence of a core hole in the final state for XMCD and its 'local character' may influence the obtained results [18]. For the case of the XMCD analysis it is discussed that if the Bruno correlation is used, systematically higher anisotropy energy values are obtained [18]. Techniques operating at different time and length scales have been used for a variety of thin-film systems. In this context we note that ferromagnetic resonance has also been used in a similar manner as XMCD for Fe/V multilayers [20]. The results of XMCD and ferromagnetic resonance have also been compared for Ni/Pt [19]. It becomes clear that several techniques may be used to obtain magnetic anisotropy energies from the anisotropy of the orbital moment and these should ultimately yield unique values. Here we base our analysis on XMCD and XRMS data. Both these techniques operate with a core hole in the final state. Though spectral areas are analysed in one case, only the dichroic contrast at a fixed photon energy is used in the other. The above-noted difference in the anisotropy energies we obtain

versus the orbital moment analysis may not be related to any XMCD specific scaling factor as proposed recently [18]; rather, the step induced anisotropy may be of mixed origin and may not depend only on magnetocrystalline effects.

As previously stated, Co on the vicinal Cu(111) surface exhibits island formation along the step edges. The lattice mismatch, of about 2% [12], has been found to result in changes in the magnetic anisotropy. The structural modifications due to the presence of step edges can be assumed to lead to tetragonal distortions along the edges of the terraces but also perpendicular to the surface in the vicinity of the steps. Due to both reduced symmetry and magneto-elastic coupling this will indeed influence the orbital moments. The correlated enhancement observed for the spin moment would, in this simplistic picture, be a consequence of a strong spin–orbit coupling. High moments for cobalt have been reported earlier. Bucher *et al* [21] reported an *internal magnetic moment* of 2.08 μ_B/atom for cobalt clusters containing 20–200 atoms. This enhancement of the magnetic moment was later confirmed by other investigators [22–24]. Our present results also allow us to correlate the *preferential growth direction* we observe here for the vicinal surface *per se* with modifications in the magnetic anisotropy observed in such surfaces. Given however the previous work on the correlation of the orbital moment anisotropy and the magnetic anisotropy [16], we cannot link the orbital moment variation observed in figure 7, interpreted as an increase in orbital moment anisotropy for the vicinal surface, with the step induced enhancement in the anisotropy constant we report here analysing the data of figure 8. We finally note that the orbital and spin moment enhancement is observed over the whole thickness range (see figure 7), much like the step induced anisotropy on vicinal surfaces [3], indicating a correlation with the island formation along the step edges we observe here. To our knowledge, the present observations have not been made earlier on a vicinal surface. Further XMCD, structural and electronic structure measurements will allow us to establish to what extent the magnetic moment increase is due to modifications in real space or electronic structure of the Co films.

5. Summary

In summary we report on Co growth on flat and vicinal Cu(111). STM investigations show that Co deposited on vicinal Cu(111) leads to a uniaxial Co island formation in the sub-monolayer thickness. But also for films above 10 ML a directed growth along a preferential direction is found. XMCD and x-ray reflectivity measurements show that the introduction of the vicinal surface also affects the value of the magnetic moment. The orbital moment m_l and the spin moment m_s for the vicinal surface are enhanced by 25% for the thickness range 1–25 ML as compared to what was found for Co on the flat surface. In addition, the 40% increase in the ratio m_l/m_s for ultrathin Co on Cu(100) reported by Tischer *et al* [4] was also found for Co on both flat and vicinal Cu(111).

Acknowledgments

This work was supported by the Swedish Research Council (Vetenskapsrådet) and the Göran Gustafsson Foundation. The authors would like to thank Erik Holmström, Sam Shallcross, Anders Bergman and Olle Eriksson for valuable discussions. Barbara Brena is to be thanked for carrying out a significant part of the experimental work. We are pleased to acknowledge the support of the whole 'Baberschke Research Group' and the particular encouragement and support of Klaus Baberschke during the STM experiments at the Freie Universität Berlin. This work was supported by the DFG, SfB290.

References

[1] de la Figuera J *et al* 1995 *Appl. Phys. Lett.* **66** 1006
[2] Berger A, Linke U and Oepen H 1992 *Phys. Rev. Lett.* **68** 839
[3] Kawakami R K *et al* 1998 *Phys. Rev.* B **58** R5924
[4] Tischer M *et al* 1995 *Phys. Rev. Lett.* **75** 1602
[5] Dürr H A *et al* 1998 *Phys. Rev.* B **58** 11853
[6] Carra P, Thole B T, Altarelli M and Xindong W 1993 *Phys. Rev. Lett.* **70** 694
[7] Arvanitis D *et al* 1996 *Spin Orbit Influenced Spectroscopies* ed H Ebert and G Schütz (Berlin: Springer) and references therein
[8] Poulopoulos P, Lindner J, Farle M and Baberschke K 1999 *Surf. Sci.* **437** 277
[9] Ebert H *et al* 1996 *Phys. Rev.* B **53** 16067
[10] Stöhr J 1995 *J. Electron Spectrosc. Relat. Phenom.* **75** 253
[11] Arvanitis D *et al* 2001 *J. Synchrotron Radiat.* **8** 120
[12] de la Figuera J, Prieto J, Ocal C and Miranda R 1993 *Phys. Rev.* B **47** 13043
[13] Gonzalez L *et al* 1981 *Phys. Rev.* B **24** 3245
[14] Le Fevre P *et al* 1995 *Phys. Rev.* B **52** 11462
[15] Hahlin A, Karis O, Hunter Dunn J and Arvanitis D 2002 *J. Appl. Phys.* **91** 6881
[16] Bruno P 1989 *Phys. Rev.* B **39** 865
[17] Cherifi S *et al* 2001 *Phys. Rev.* B **64** 184405
[18] Dhesi S, van der Laan G, Dudzik E and Shick A 2001 *Phys. Rev. Lett.* **87** 067201
[19] Wilhelm F *et al* 2000 *Phys. Rev.* B **61** 8647
[20] Anisimov A *et al* 1999 *Phys. Rev. Lett.* **82** 2390
[21] Bucher J, Douglass D and Bloomfield L 1991 *Phys. Rev. Lett.* **66** 3052
[22] Douglas D, Cox A, Bucher J and Bloomfield L 1993 *Phys. Rev.* B **47** 12874
[23] Respaud M *et al* 1998 *Phys. Rev.* B **57** 2925
[24] Mlynarski P *et al* 1999 *Vacuum* **54** 143